Advances in Science and Technology Research Journal

Advances in Science and Technology Research Journal 2024, 18(2), 226–237
https://doi.org/10.12913/22998624/184152
ISSN 2299-8624, License CC-BY 4.0

Received: 2023.12.11
Accepted: 2024.02.15
Published: 2024.03.14

Screw Extrusion as a Scalable Technology for Manufacturing Polylactide Composite with Graphene Filler

Daniel Kaczor[1,2*], Krzysztof Bajer[2], Aneta Raszkowska-Kaczor[2], Oksana Krasinska[2], Grzegorz Domek[2], Paweł Szroeder[3]

[1] Faculty of Mechatronics, Kazimierz Wielki University, ul. Kopernika 1, 85-074 Bydgoszcz, Poland
[2] Łukasiewicz Research Network – Institute for Engineering of Polymer Materials and Dyes, ul. Marii Skłodowskiej-Curie 55, 87-100 Toruń, Poland
[3] Faculty of Physics, Kazimierz Wielki University, ul. Powstańców Wielkopolskich 2, 85-090 Bydgoszcz, Poland
* Corresponding author's e-mail: kaczor.daniel.piotr@gmail.com

ABSTRACT

The use of carbon nanomaterials as fillers in the process of obtaining polymer composites by extrusion poses many problems. The high agglomeration ability and low bulk density of carbon nanomaterials do not allow to easy production of composites characterized by very good dispersion of the filler in the polymer matrix, which is required to obtain a high-quality product. The advantage of this type of fillers is that the improvement of the composite properties can be achieved even at a low degree of filling. In this article, we describe a method for obtaining polylactide composites with a nanofiller in the form of graphene nanoplatelets. To overcome the difficulties associated with the use of graphene, we divided the process of obtaining composites into two stages. In the first stage, we made a masterbatch containing 25 wt.% graphene, from which, in the second stage, we obtained target composites containing from 0.1 to 2 wt.% graphene. A twin-screw extruder was used in both stages. The tested filling levels had no significant impact on the recorded processing parameters. The composites obtained by the described method are characterized by good dispersion of graphene. However the graphene agglomerates can be observed in the polymer matrix. Composites were tested by SEM, FTIR, DSC and MFR methods. Mechanical tests such as static tension, three-point bending, impact strength showed that the addition of 0.5 wt.% of graphene improves tensile strength by 10%, Young's modulus by 19% and both flexural strength and flexural modulus by 15%. The carbon filler has an impact on crystallization process of the polymer matrix by acting as a nucleating agent.

Keywords: polylactide, composite, masterbatch, graphene, extruder.

INTRODUCTION

The last decade has seen a surge of interest in biopolymers, which is related to the unresolved issue of disposal of products made from plastics produced from fossil fuel derivatives. Replacing conventional plastics with biopolymers made from renewable organic materials is therefore one of the biggest technological challenges. Product design now considers the life cycle – from manufacture to disposal. From this point of view, its ability to biodegrade after use is crucial. Not all biopolymers are biodegradable (e.g. biopolyethylene), nor are all biodegradable biopolymers derived from renewable organic materials (e.g. polycaprolactone) [1]. One of the bidegradable polymers of biological origin is polylactide, first synthesized in 1932 by DuPont employee Wallace Carothers by heating lactic acid under vacuum [2]. Among the advantages of polylactide, in addition to its biodegradability, are its good mechanical properties. The disadvantages are low impact resistance, susceptibility to thermal deformation and low gas barrier [3].

Currently, polylactide occupies a leading role on the biodegradable polymers market [4]. Since

1960, it has been used in medicine and pharmacy as absorbable implants, sutures and in controlled drug release [5, 6]. Currently, it is used in many industries: automotive [7, 8], agriculture [9, 10], medicine [11, 12], electronics [13, 14], packaging [15, 16] and others. Broader use of polylactide requires modification of its properties by adding natural [17, 18] or synthetic fibres [19], biodegradable polymers [20] or other fillers [21, 22].

In 2004, C. Berger et al. [23] and K. Novoselov et al. [24] independently reported obtaining a two-dimensional graphene by epitaxial growth and mechanical graphite exfoliation, respectively. The concept of graphene as a single layer of graphite was proposed as early as 1984 by Boehm [25], who built on the theoretical work of Walles [26]. In 2010 Andre Geim and Konstantin Novoselov were Nobel Prize awarded "for groundbreaking experiments regarding the two-dimensional material graphene" [27]. Thanks to its excellent mechanical properties, graphene is also used as an additive in polylactide composites.

Graphene is a 2D crystal composed of the covalently bonded sp^2 carbon atoms arranged in honey-comb crystalline lattice [28]. Covalent σ bonds are responsible for extraordinary mechanical properties of graphene, the Young's modulus of 1 TPa and an instrinsic strength of 130 GPa [29]. These properties, combined with high thermal conductivity above 3000 W/(m·K) [30], excellent gas barrier [31] or the ability to withstand extremely high electric current densities (a million times greater than copper) [32], make graphene a good candidate as a filler in polymer composites.

One of the biggest challenges of the technology of manufacturing polymer composites with graphene filler is to achieve a good dispersion of graphene in the polymer matrix. Various approaches are used to achieve good graphene dispersion. In polymerization *in situ*, monomers intercalate between graphene layers, followed by polymerization [33]. In the mixing-in-solution method, the polymer is dissolved in a solvent, then graphene filler is added. Polymer macromolecules in solution easily intercalate between graphene layers. After evaporation of the solvent, a composite with well-dispersed filler is obtained [34]. Both approaches ensure good incorporation of graphene into the structure of the polymer; however, they are difficult to apply on a scale larger than the laboratory scale. The only method that allows the development of industrial technology for the production of graphene-filled composites is melt blending using single- twin-screw extruders [35].

In the article, we describe the process of preparing samples of polylactide composites containing from 0.1 to 2 wt.% of graphene. The target composites are obtained from our own masterbatch containing 25 wt.% of graphene. The use of a masterbatch improves the composite production process by significantly facilitating the dosing of the nanomaterial. We examined the obtained composites in terms of filler dispersion in the matrix, possible changes in the chemical structure of the polymer matrix, the influence of graphene content on the melt flow rate, thermal and mechanical properties of the composites.

MATERIALS AND METHODS

Materials

As a polymer matrix polylactide produced by Total-Corbion (Gorinchen, Netherlands) with the trade name Luminy® LX175 was used. Basic properties of used polylactide: density of 1.24 g/cm^3, stereochemical purity 96% (L-isomer), glass and melting temperature of 60 °C and 155 °C respectively. For masterbatches containing 25 wt% graphene, a polymer in powder form with a size ranging from 100 to 600 μm was used. The composites were made of polylactide in the form of granules.

Graphene nanoplatelets (GNP) were provided by The Institute of Carbon Technologies (Toruń, Poland). The thickness of the used GNPs is 3 nm, diameter 1.5 μm, specific surface area 800 m^2/g.

Composite production technology

The composite production process consisted of two stages:

- first stage: obtaining a polylactide masterbatch containing 25 wt.% graphene from polylactide in powder form with a size from 100 to 600 μm
- second stage: obtaining target composites containing from 0.1 to 2.0 wt.% graphene using the masterbatch obtained in the first stage and polylactide in granules form.

Before extrusion, both the masterbatch and the composites, all ingredients were dried in POL-EKO SLW 180 STD dryer (POL-EKO sp.k., Poland) at 80 °C for 8 hours.

Masterbatch preparation – first stage

Premixed PLA in powder form with 25 wt.% GNP was used to obtain the masterbatch by extrusion. Twin-screw Bühler BTSK (Switzerland) co-extruder with a screw diameter of 20 mm and a L/D (length to diameter) of 40 was used. Used configuration included four zones responsible for mixing and grinding the molten material (Fig. 1). In the first zone were two kneading elements – KBW 90/2/15 and KBW 45/5/20. The subsequent zones contained elements, whose task was to retain the melt in the mixing zone for a longer time. The reverse mixing and grinding segments present in this zone are responsible for this. The screw system used is characterized by good mixing and grinding properties intensified by the presence of reverse elements. The masterbatch was extruded at a speed of 100 rpm using the temperature profile: 170 °C (Zone 1), 175 °C (Zone 2), 180 °C (Zone 3), 185 °C (Head).

Composite preparation – second stage

The masterbatch obtained in the first stage was used to produce composites. For this purpose, the appropriate amount of masterbatch, required to obtain composites with carbon filler from 0.1 wt.% to 2.0 wt.%, was mixed with polylactide in the form of granules. The material was then extruded at a speed of 150 rpm and in temperatures of 170 °C (Zone 1), 175 °C (Zone 2), 180 °C (Zone 3), 185 °C (Zone 4), 180 °C (Head), using the same extruder and plasticizing system which one was used to receiving masterbatch. As a result, composites containing: 0.1 wt.% GNP, 0.3 wt.% GNP, 0.5 wt.% GNP, 1.0 wt.% GNP, 2.0 wt.% GNP were obtained, which were marked respectively as: 0.1% GNP/PLA, 0.3% GNP/PLA, 0.5% GNP/PLA, 1.0% GNP/PLA, 2.0% GNP/PLA. The composites were compared with a sample without the addition of graphene, which was also subjected to the same extrusion process as the composites. This sample was named PLA.

Material characterization

Microscopic analysis

A Hitachi SU8010 (Japan) scanning electron microscope (SEM) was used to evaluate the dispersion, presence of agglomerates and uniformity of distribution of the graphene filler in the polymer matrix. The pictures were taken after coating a thin layer of gold onto the surface of the samples in order to increase its electrical conductivity, at an acceleration voltage of 10 kV.

FTIR-ATR analysis

Fourier transform infrared spectrometer Cary 630, Agilent Technology, Santa Clara, CA, USA coupled with attenuated total reflectance module equipped with diamond crystal was used for recording of infrared absorption spectra in the range of 400–4000 cm^{-1} , with resolution 2 cm^{-1} and signal to noise ratio (1 min, RMS) 30000:1.

Thermal behaviour analysis

The differential scanning calorimetry (DSC) technique was used to assess the impact of the extrusion process and the addition of graphene on the thermal properties of the composites. Thermograms were recorded using a Mettler Toledo DSC1 calorimeter. The measurement was carried out in three stages: two heats and one of cooling, separated by two isothermal stages. In the first stage - Heating 1, the sample was heated at a rate of 10 °C/min from 0 °C to 300 °C. Then the sample was kept at a temperature of 300 °C for 5 min. After this isothermal step, the sample was cooled at a rate of 10 °C/min to 0 °C. Cooled sample was

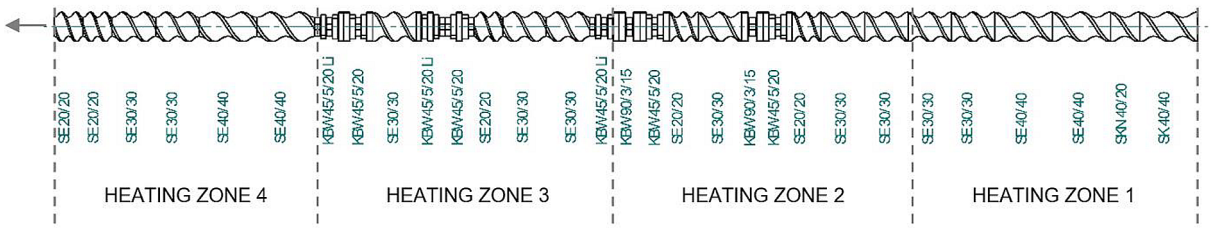

Fig. 1. Screw configuration with marked heating zones of extruder, SK - feeding segments, SE - conveying segments, KBW - kneading elements, elements marked as Li - backward elements, numbers encode: angle (KBW only)/step/length in mm

kept at 0 °C for 5 min. Then was heated again - Heating 2, at a rate of 10 °C/min from 0 °C to 300 °C. Measurements were made in an inert atmosphere – nitrogen (gas flow over the sample 60 cm^3/min). Samples sealed in aluminum crucibles weighing 5 to 7 mg were used. The percentage of the crystalline phase in the polymer was calculated using the equation [36]:

$$X_C = \left(\frac{\Delta H_m - \Delta H_{cc}}{w \Delta H_m^0} \right) \cdot 100\% \qquad (1)$$

where: ΔH_m – melting enthalpy (J/g); ΔH_{cc} – cold crystallization enthalpy (J/g); ΔH^0_m – melting enthalpy of 100% crystalline PLA (93 J/g [37]); w – fraction of the polymer in the composite materials. The analysis was performed in agreement with ISO 11357-(1–3) standards [38]. The accuracy of temperature determination was ± 0.8 °C and enthalpy ± 0.5 J/g.

Melt flow rate

A Dynisco LMI 4003 capillary plastometer was used to determine the mass flow rate (MFR) of the composites. The measurement was performed in accordance with the PN-EN ISO 1133 standard [39]. Measurement conditions: temperature 190 °C, piston load 2.16 kg, melting time 300 s, cutting time 10 s. Before measurement, the composite samples were dried for 4 hours at 80 °C.

Mechanical tests

Before performing the tests, the samples were conditioned for at least 24 hours at a temperature of 23 ± 1 °C and a humidity of 50 ± 5%. Mechanical tests were also carried out under the same climatic conditions.

The specimens for mechanical tests were made using the injection technique in agreement with PN-EN ISO 294-1 standard [40]. Two types of samples were prepared: shapes in the 1A mold ("dog bone" shape, 2 mm of thickness, for tensile strength tests) and beams (length/width/thickness – 80/10/4 mm, for three-point bending and Charpy test). Specimens were made with Battenfeld Plus 35/75 UNILOG B2 injection molding machine with three heating zones, screw diameter of 22 mm and L/D 17. Injection parameters: processing temperature 185 °C (all heating zones), dosing speed 150 rpm, dosing back pressure 232 Bar, injection pressure 1627 Bar, screw rotation speed in the injection phase from 126 (start of injection) to 210 rpm (end of injection), pressure mold closure 1627 Bar, pressing time 35 sec, cooling time 20 sec, mold temperature 40 °C, injection volume 28.8 cm^3 for 1A specimens and 20.8 cm^3 for bars. Before injection, the composites were dried for 4 hours at 80 °C.

The TIRAtest 27025 (TIRA Maschinenbau GmbH, Germany) testing machine was used to measure mechanical properties of samples in static tension. The tests was made in accordance with PN-EN ISO 527-(1-2) standard [41]. Testing machine was , equipped with a 3 kN measuring head. Measurement parameters: Test speed: 1.0 mm/min to determine the modulus and 50 mm/min for other measured parameters, gauge length: 50 mm. According to standard, means were calculated from five replicates. The TIRAtest 27025 testing machine was also used to perform three-point bending tests. Measurements were made with use a 3 kN measuring head, support spacing 64 mm and testing speed 2 mm/min. Five replicates were tested for each sample and the average values were reported.

IMPats-15/50 test stand (ATSFAAR S.p.A., Italy) was used to perform Charpy impact tests. Measurements were made with accordance to PN-EN ISO 179-1 [42] standard. Hammer used to break the specimens had impact energy 1 J and velocity at impact of 2.90 m/s. Notched using NOTCH VIS (CEAST) machine samples in a shape 1eA, with 8 mm width under notch, was measure. After notching, specimens were conditioning by at least 16 hours in standard conditions. Ten replicates were tested ror each sample.

RESULTS

Extrusion process analysis

During the extrusion of the composites, the following parameters were recorded: stock temperature (T_t), main drive torque (M_0), power main drive (W), and efficiency (Y). Parameters values are show in Table 1. Extruded composites in the form of granules were characterized by a smooth, shiny surface. No major differences were found in the recorded process parameters between individual samples containing graphene. There are slight differences between the pure polylactide sample and the composites. Unfunctionalized GNP plates produce hydrodynamic slip and alignment in the shear flow direction, causing a decrease in the viscosity of the composites and thus reducing processing resistance [43].

Table 1. Parameters recorded during extrusion

Sample	PLA	0.1% GNP/PLA	0.3% GNP/PLA	0.5% GNP/PLA	1.0% GNP/PLA	2.0% GNP/PLA
T_t [°C]	210	200	200	205	203	202
M_o [Nm]	21.5	20.2	21.1	20.1	20.2	20.2
W [kW]	0.63	0.61	0.61	0.60	0.61	0.60
Y [kg/h]	3.25	3.12	3.12	3.12	3.12	3.12

Microscopic analysis

Figure 2 contains SEM images of original GNP agglomerates, the fracture surface of PLA masterbatch granules containing 25 wt.% GNP and individual composite samples.

The morphology of raw materials is consistent with the data provided by suppliers. Polylactide powder consists of grains ranging in size from 100 to 600 μm (Figure 2a), GNPs occur in the form of agglomerates composed of graphene plates (Figure 2b). On the crack surface of the GNP/PLA masterbatch filler agglomerates are visible (Figure 2c). The cracked surface of pure PLA (Figure 2d) is smooth, indicating the inherent brittleness and stiffness of the material. GNP agglomerates and smaller graphene structures are also visible in photos of the fracture surfaces of composite samples (Fig. 2e–f). SEM photos indicate that GNP is evenly dispersed in the polymer matrix, but we did not avoid its agglomeration during extrusion. The presence of agglomerates indicates strong interactions between graphene nanoplatelets, which could not be overcome both after twice extruding the masterbatch and after subsequent extrusion of the target composites. No defects were observed in the structure of the polymer matrix in the form of pores, cracks or other discontinuities.

FTIR-ATR analysis

Figure 3 show a comparison of the FTIR-ATR composites and PLA recorded spectra. All recorded spectra contain bands characteristic of polylactide. The crystalline and amorphous polymer phases are represented by bands located at 754 cm^{-1} and 865 cm^{-1} respectively [44]. At 1041 cm^{-1} appears stretching modes of C-CH_3 groups.

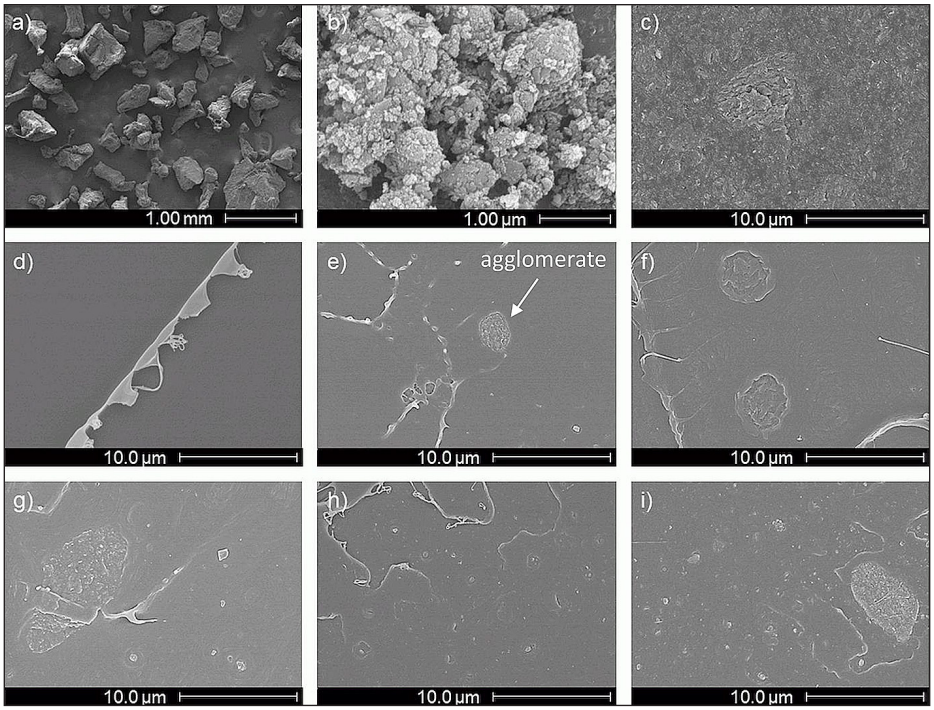

Fig. 2. SEM picture of: (a) PLA powder, (b) GNPs, (c) fracture surface of GNP/PLA masterbatch, (d) fracture surface of the extruded neat PLA, (e-i) fracture surface of the extruded GNP/PLA composite containing 0.1, 0.3, 0.5, 1.0 and 2.0 wt.% of GNP, respectively

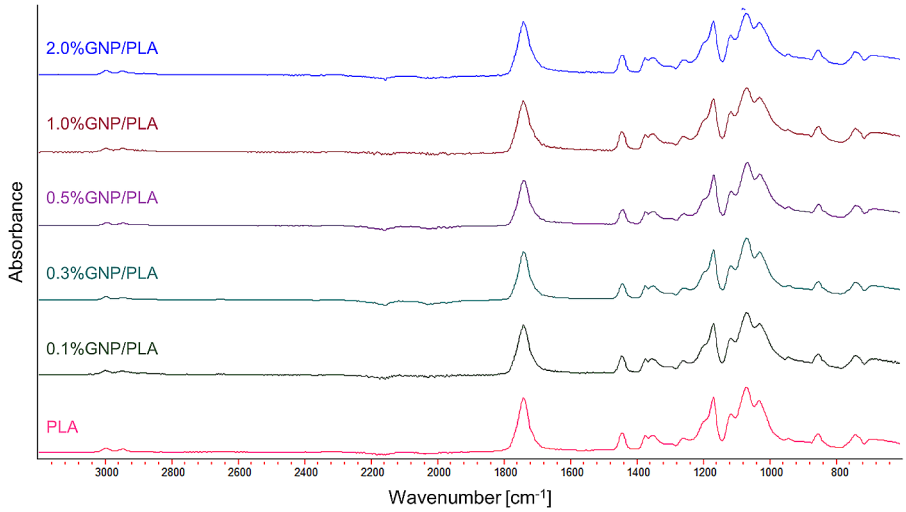

Fig. 3. FTIR-ATR spectra of the tested samples and original polylactide

C-O-C symmetric stretching modes can be found at 1080 cm^{-1} and asymmetric at 1179 and 1266 cm^{-1}. Rocking modes of CH_3 groups are visible at 1127 cm^{-1}. Symmetric bending modes of CH and CH_3 appear at 1358 and 1381 cm^{-1}. At 1450 cm^{-1} asymmetric bending modes of CH and CH_3 groups can be found. The C=O ester stretching modes occur at 1747 cm^{-1}. Low intensity bands at 2944 and 2995 cm^{-1} are assigned to the asymmetric stretching modes of CH_3 [45,46]. The spectra of samples containing GNP do not differ from each other and from spectrum of pure polylactide.

Reducing the intensity of the bands assigned to C=O (1747 cm^{-1}) and C-O-C group (1080 cm^{-1}, 1179 cm^{-1}) was not observed. Changes in this bands may by a result of the shortening of the polymer chain [47]. This proves that the applied that the addition of graphene filler did not cause degradation of the polymer matrix or their impact was minimal.

Thermal behaviour analysis

Recorded temperature values of: T_g – glass transition, T_{cc} – cold crystallization, T_m – melting point, enthalpy of: ΔH_{cc} – cold crystallization, ΔH_m – melting enthalpy are shown in Table 2, thermograms of first and second heating on Figures 4 and 5. In the thermograms of the first heating, used to erase the thermal history of the sample after the extrusion process, the first endothermic transition can be seen around the temperature of 60 °C. The

Table 2. Thermal parameters obtained by DSC

Sample	PLA	0.1% GNP/PLA	0.3% GNP/PLA	0.5% GNP/PLA	1.0% GNP/PLA	2.0% GNP/PLA
Heating 1						
T_g^1 [°C]	60.0	61.6	61.0	61.7	61.7	61.9
T_{cc}^1 [°C]	111.1	123.8	130.0	-	-	-
ΔH_{cc}^1 [J/g]	26.0	21.2	4.9	-	-	-
T_m^1 [°C]	151.6	154.6	155.6	154.6	154.7	155.6
ΔH_m^1 [J/g]	26.1	21.8	7.2	22.9	25.8	26.9
X_c^1 [%]	0	0	2.5	24.9	27.9	29.5
Heating 2						
T_g^2 [°C]	59.6	59.3	59.4	59.0	58.9	58.8
T_{cc}^2 [°C]	129.2	126.4	129.7	129.8	124.6	129.2
ΔH_{cc}^2 [J/g]	9.5	18.7	3.7	3.5	16.3	8.4
T_m^2 [°C]	150.0	148.8	149.8	149.3	147.5	149.3
ΔH_m^2 [J/g]	9.5	18.9	3.7	3.4	17.0	8.3
X_c^2 [%]	0	0	0	0	0	0

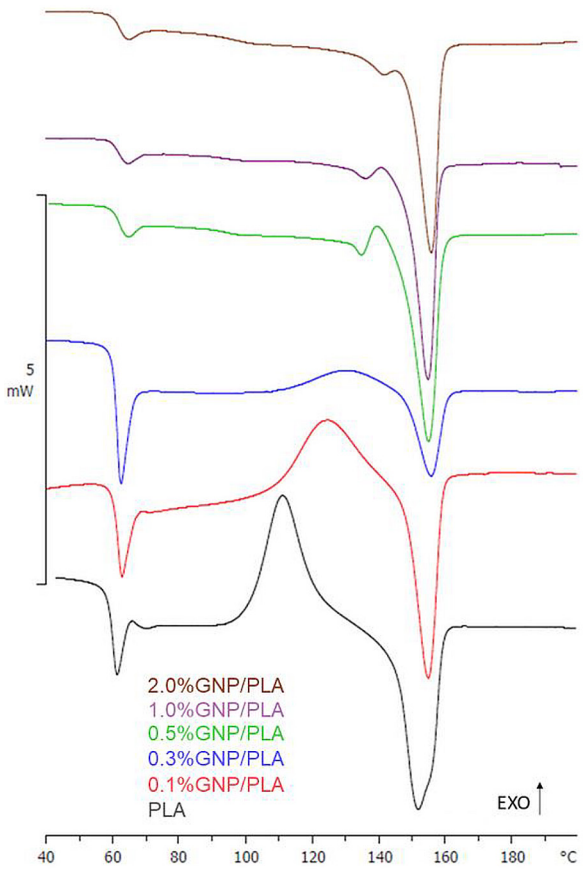

Fig. 4. Heating 1 DSC thermograms of samples

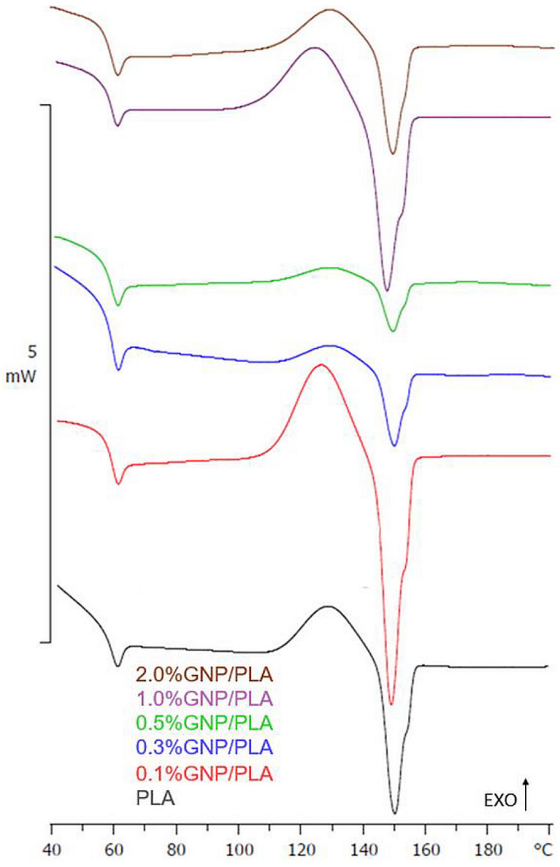

Fig. 5. Heating 2 DSC thermograms of samples

temperature of this transition is called the glass transition temperature. After exceeding this temperature, the polymer chains become movable. For samples containing GNP, this temperature is approximately 1–2 °C higher than for sample without filler. The increase in temperature is caused by the limitation of the movement of polymer chains by GNPs [48].

Cold crystallization was recorded for the PLA sample and composites containing 0.1 and 0.3 wt.% GNP. The temperature of this transition for these samples increased with the increase in the amount of filler. This effect is related to the negative impact of the filler on the mobility of the polylactide chains [14]. Changes in the enthalpy of this process are also visible. $\Delta H_{cc}{}^{1}$ decreases with increasing filling of the composites until this process is completely inhibited for samples containing 0.5 wt.% and more GNP. The presence of the filler limits the space in which crystallites can grow. This results in the formation of small, imperfect crystallites whose T_{cc} is higher and ΔH_{cc} is lower compared to more perfect structures [15]. For composites containing 0.5 wt.% or more of GNPs, no cold crystallization process was observed. This may mean that GNPs induce the formation of crystallites during the process of obtaining composites. As a result, composites with a higher degree of crystallinity are created [49]. $X_c{}^{1}$ increases with increasing filler content to the level 29.5% for 2.0% GNP/PLA sample. The melting temperature recorded during the Heating 1 of the composite samples is approximately 3–4 °C higher in comparison to PLA sample. Which is related to the melting of a larger number of crystals in the samples containing graphene, which were created due to the nucleating effect of GNPs [50].

During cooling, no transitions related to polymer crystallization were recorded. Which means that crystallites can only form when heated in a molten form of polymer. Polylactide chains were not able to reorganize into a more ordered form in the solid phase [51]. The glass transition temperature recorded during Heating 2 for all samples had a similar value. This indicates that the filler had little effect on the mobility of the polymer chains [52]. No relationship was observed between the temperature and enthalpy of cold crystallization and GNPs

content in composites. The melting peaks of all samples recorded during the second heating are not symmetrical. The asymmetry of the peak is caused by the effect of the presence of two types of crystallites differing in size in the samples, or by a disorder [53]. The lower temperature melting peak is attributed to the melting of imperfect crystallites and its recrystallization to more stable form. The newly formed crystallites melt at a higher temperature [54]. All samples showed in second heat amorphous character.

Melt flow rate

Composites and reference sample melt flow rate values are show in Table 3. Information about melt viscosity can be obtained by measuring the melt flow rate. It is a measurement performed at a specific, standardized temperature and piston load, during which the mass of molten material flowing through a standardized capillary is measured in a given time unit. In this approach, the MFR can be considered as an extrusion rheometer representing a specific point on the shear stress versus shear rate curve [55, 56]. The MFR value of pristine polylactide used to prepare composite and the reference sample was 3 g/10 min. Because the increase in the MFR value may be caused by the degradation of the polymer related to the shortening and disruption of its chains during processing with an extruder [57, 58]. Contrary to the used polymer processing conditions, the addition of GNP to the composites had no effect on the polymer degradation.

Mechanical tests

Tensile strength – σ_m, stress at brake – σ_b, strain at strength – ε_m, strain at break – ε_b, tensile modulus, modulus of elasticity under tension (young's modulus) – E_t, were determined and shown in Table 4. The addition of GNP to the polymer matrix resulted in an increase in both the σ_m and E_t, without a significant change in the elongation values of the samples. The highest values were obtained for the sample containing 0.5 wt% GNP. For this sample σ_m increased by 10% and E_t by 19% compared to a sample extruded under the same conditions but without the addition of graphene. All samples showed typical brittle fracture behaviour, without any visible yielding phenomenon. The very good strength parameters of GNP are responsible for improving the mechanical properties [59]. Additionally, the large specific surface area of GNP facilitates transfer of stresses through filler-polymer interface [60]. Most of the external loads are carried by the PLA matrix. Microcracks created during stretching initiate and spread in the polymer matrix of composites when the applied load exceeds its strength [61]. The increase in the number of defects in the continuity of the polymer matrix related to the increased number of graphene platelets agglomerates may be responsible for the decrease in mechanical properties of composites filled above 0.5 wt% GNP [62].

In three-point bending tests flexural strength – σ_{fM}, flexural strain at flexural strength – ε_{fM}, flexural stress at conventional deflection – σ_{fc},

Table 3. Composites and reference sample MFR values (standard deviation)

Sample	PLA	0.1% GNP/PLA	0.3% GNP/PLA	0.5% GNP/PLA	1.0% GNP/PLA	2.0% GNP/PLA
MFR [g/10 min]	7.07 (0.05)	7.51 (0.06)	7.41 (0.09)	7.44 (0.13)	7.41 (0.10)	7.62 (0.05)

Table 4. Mechanical properties – static tension (standard deviation)

Sample	PLA	0.1% GNP/PLA	0.3% GNP/PLA	0.5% GNP/PLA	1.0% GNP/PLA	2.0% GNP/PLA
σ_m [MPa]	62.5 (0.7)	64.6 (0.5)	67.1 (0,8)	69.0 (1.0)	68.0 (0.5)	65.9 (0.9)
σ_b [MPa]	60.8 (1.0)	62.6 (2.0)	65.6 (0.3)	68.8 (1.3)	67.8 (0.4)	64.7 (2.3)
ε_m [%]	4.2 (0.2)	3.9 (0.1)	4.1 (0.1)	3.9 (0.1)	3.9 (0.1)	3.7 (0.1)
ε_b [%]	4.5 (0.2)	4.3 (0.2)	4.3 (0.2)	4.0 (0.1)	3.9 (0.1)	3.8 (0.2)
E_t [MPa]	1982 (62)	1966 (149)	2177 (16)	2366 (43)	2333 (109)	2306 (109)

Table 5. Mechanical properties – three-point bending (standard deviation)

Sample	PLA	0.1% GNP/PLA	0.3% GNP/PLA	0.5% GNP/PLA	1.0% GNP/PLA	2.0% GNP/PLA
σ_{fm} [MPa]	97.0 (2.8)	101.4 (2.2)	106.9 (2.4)	111.8 (4.2)	110.2 (0.3)	108.8 (2.8)
σ_{fc} [MPa]	95.2 (2.6)	99.0 (2.4)	105.0 (3.0)	111.7 (5.3)	109.9 (0.6)	107.4 (4.0)
ε_{fm} [%]	4.3 (0.1)	4.5 (0.2)	4.4 (0.5)	3.9 (0.8)	3.8 (0.1)	4.0 (0.8)
E_f [MPa]	3290 (181)	2908 (143)	3075 (129)	3709 (261)	3444 (202)	3317 (44)

Table 6. Mechanical properties – impact strength (standard deviation)

Sample	PLA	0.1% GNP/PLA	0.3% GNP/PLA	0.5% GNP/PLA	1.0% GNP/PLA	2.0% GNP/PLA
a_{cN} [kJ/m^2]	2.73 (0.29)	3.05 (0.37)	3.43 (0.41)	3.41 (0.26)	3.47 (0.46)	3.46 (0.33)

modulus of elasticity in flexure, flexural modulus – E_f were measured and show in Table 5.

In three-point bending results, a slight increase in the strength of GNP composites can be observed. The best results were obtained again for the sample containing 0.5 wt% GNP. For this sample, the σ_{fm} and E_f increased by 15% in comparison to PLA sample. The deterioration of properties after exceeding 0.5 wt.% of filling is caused by an increase in the number of agglomerates in the composite samples, what was seen also in tensile strength tests [63]. Table 6 shows the impact strength values determined by the Charpy method (a_{cN}).

The addition of GNP to the composites did not significantly change the impact strength values of the samples. Although a slight improvement in this parameter is visible, but it is so small that it is more accurate to say that this parameter did not deteriorate after adding GNP to the polymer matrix.

CONCLUSIONS

Dividing the production process of polylactide composites with nano graphite plates into two stages made it much easier. However, the used configuration of the extruder plasticizing system did not allow for the complete elimination of the presence of GNP agglomerates in the composite. The increase in GNP filling in the composites did not have a major impact on the extrusion parameters of the composites. A slight decrease in the generated loads and stock temperature was noticed compared to the sample without the addition of filler. The difference is caused by the decrease in melt viscosity caused by the presence of GNP which is confirmed by the MFR study.

Despite extruding the highly filled GNP masterbatch twice, the presence of graphene agglomerates was still found in it. Agglomerates were also found in SEM photos of the composites, which indicates strong interactions between graphene flakes. In the pictures of the masterbatch, sample without the addition of filler and composites any discontinuities or pores in the polymer matrix were found. The presence of voids and pores, resulting from the appearance of CO or CO_2 in the system, may indicate polymer degradation [64].

The results of the FTIR-ATR analysis indicate that the addition of GNP during sample preparation did not cause any changes in the chemical structure of the polymer matrix. The analysis of DSC thermograms allows us to conclude that GNP supports the crystallization process of polylactide. However, due to the limited mobility of the polymer chains by the presence of the filler, the crystallites formed were small and imperfect. An increase in the degree of crystallinity of composites with graphene may affect the value obtained during mechanical tests. Polymers with a more crystalline structure are more durable but also more brittle [65].

The presence of GNP did not have a major impact on the measured melt flow rate. However, the extrusion conditions used resulted in partial degradation of the polymer matrix, which resulted in an increase in the MFR value compared to the data provided by the polylactide manufacturer.

GNP had the greatest impact on the properties of the obtained composites on the results of mechanical tests. Where their small addition (0.5

wt.%) resulted in an increase in tensile strength by 10% and young's modulus by 19% and flexural strength and flexural modulus by 15%, without deterioration of the other measured parameters.

Acknowledgments

This work is supported by the Ministry of Education and Science of The Republic of Poland as part of the 'Implementation doctorate' program (contract No. DWD/4/71/2020) and by the Faculty of Mechatronics of The Kazimierz Wielki University (funds from the subsidy for scientific research).

REFERENCES

1. Babu RP, O'Connor K, Seeram R. Current progress on bio-based polymers and their future trends. Prog Biomater. 2013; 2(1): 8.
2. Carothers WH, Dorough GL, Natta FJV. Studies of polymerization and ring formation. The reversible polymerization of six-membered cyclic esters. J am chem soc. 1932; 54(2): 761–72.
3. Trivedi AK, Gupta MK, Singh H. PLA based biocomposites for sustainable products: A review. Advanced Industrial and Engineering Polymer Research. 2023; 6(4): 382–95.
4. Androsch R, Schick C, Di Lorenzo ML. Kinetics of nucleation and growth of crystals of poly(l-lactic acid). Advances in Polymer Science. 2018; 279: 235–272.
5. Kawai F. Polylactic Acid (PLA)-degrading microorganisms and PLA depolymerases. ACS Symposium Series. 2010; 1043: 405–414.
6. Avinc O, Khoddami A. Overview of poly(lactic acid) (PLA) fibre. Fibre Chem. 2009; 41(6): 391–401.
7. Prasanth SM, Kumar PS, Harish S, Rishikesh M, Nanda S, Vo DVN. Application of biomass derived products in mid-size automotive industries: a review. Chemosphere. 2021; 280: 130723.
8. Barillari F, Chini F. Biopolymers - sustainability for the automotive value-added chain. ATZ Worldw. 2020; 122(11): 36–39.
9. Knoch S, Pelletier F, Larose M, Chouinard G, Dumont MJ, Tavares JR. Surface modification of PLA nets intended for agricultural applications. Colloids and Surfaces A: Physicochemical and Engineering Aspects. 2020; 598: 124787.
10. Fahim IS, Chbib H, Mahmoud HM. The synthesis, production & economic feasibility of manufacturing PLA from agricultural waste. Sustainable Chemistry and Pharmacy. 2019; 12: 100142.
11. DeStefano V, Khan S, Tabada A. Applications of PLA in modern medicine. Engineered Regeneration. 2020; 1: 76–87.
12. Davachi SM, Kaffashi B. Polylactic acid in medicine. Polymer-Plastics Technology and Engineering. 2015; 54(9): 944–967.
13. Mattana G, Briand D, Marette A, Vásquez Quintero A, de Rooij NF. Polylactic acid as a biodegradable material for all-solution-processed organic electronic devices. Organic Electronics 2015; 17: 77–86.
14. Shi X, Dai X, Cao Y, Li J, Huo C, Wang X. Degradable poly(lactic acid)/metal–organic framework nanocomposites exhibiting good mechanical, flame retardant, and dielectric properties for the fabrication of disposable electronics. Ind Eng Chem Res. 2017; 56(14): 3887–3894.
15. Shao L, Xi Y, Weng Y. Recent advances in PLA-based antibacterial food packaging and its applications. Molecules. 2022; 27(18): 5953.
16. Swetha TA, Bora A, Mohanrasu K, Balaji P, Raja R, Ponnuchamy K. A comprehensive review on polylactic acid (PLA) – synthesis, processing and application in food packaging. International Journal of Biological Macromolecules. 2023; 234: 123715.
17. Siakeng R, Jawaid M, Ariffin H, Sapuan SM, Asim M, Saba N. Natural fiber reinforced polylactic acid composites: a review. Polymer Composites. 2019; 40(2): 446–463.
18. Rajeshkumar G, Arvindh Seshadri S, Devnani GL, Sanjay MR, Siengchin S, Prakash Maran J. Environment friendly, renewable and sustainable poly lactic acid (PLA) based natural fiber reinforced composites – a comprehensive review. Journal of Cleaner Production. 2021; 310: 127483.
19. Sun Y, Zheng Z, Wang Y, Yang B, Wang J, Mu W. PLA composites reinforced with rice residues or glass fiber—a review of mechanical properties, thermal properties, and biodegradation properties. J Polym Res. 2022; 29(10): 422.
20. Olaiya NG, Surya I, Oke PK, Rizal S, Sadiku ER, Ray SS. Properties and characterization of a PLA–chitin–starch biodegradable polymer composite. Polymers. 2019; 11(10): 1656.
21. Fu Z, Cui J, Zhao B, Shen SGF, Lin K. An overview of polyester/hydroxyapatite composites for bone tissue repairing. Journal of Orthopaedic Translation. 2021; 28: 118–130.
22. Shahdan D, Rosli NA, Chen RS, Ahmad S, Gan S. Strategies for strengthening toughened poly(lactic acid) blend via natural reinforcement with enhanced biodegradability: a review. International Journal of Biological Macromolecules. 2023; 251: 126214.
23. Berger C, Song Z, Li T, Li X, Ogbazghi AY, Feng R. Ultrathin epitaxial graphite: 2D electron gas properties and a route toward graphene-based nanoelectronics. J Phys Chem B. 2004; 108(52):

19912–19916.

24. Novoselov KS, Geim AK, Morozov SV, Jiang D, Zhang Y, Dubonos SV. Electric field effect in atomically thin carbon films. Science. 2004; 306(5696): 666–669.
25. Boehm HP, Setton R, Stumpp E. Nomenclature and terminology of graphite intercalation compounds. Carbon. Pergamon. 1986; 24: 241–245.
26. Wallace PR. The band theory of graphite. Phys Rev. 1947; 71(9): 622–634.
27. Gerstner E. Nobel Prize. Andre Geim & Konstantin Novoselov. Nature Phys. 2010; 6(11): 836–836.
28. Duplock EJ, Scheffler M, Lindan PJD. Hallmark of perfect graphene. Phys Rev Lett. 2004; 92(22): 225502.
29. Morozov SV, Novoselov KS, Katsnelson MI, Schedin F, Elias DC, Jaszczak JA. Giant intrinsic carrier mobilities in graphene and its bilayer. Phys Rev Lett. 2008; 100(1): 016602.
30. Balandin AA. Thermal properties of graphene and nanostructured carbon materials. Nature Mater. 2011; 10(8): 569–581.
31. Bunch JS, Verbridge SS, Alden JS, van der Zande AM, Parpia JM, Craighead HG. Impermeable atomic membranes from graphene sheets. Nano Lett. 2008; 8(8): 2458–2462.
32. Moser J, Barreiro A, Bachtold A. Current-induced cleaning of graphene. Applied Physics Letters. 2007; 91(16): 163513.
33. Norazlina H, Kamal Y. Graphene modifications in polylactic acid nanocomposites: a review. Polym Bull. 2015; 72(4): 931–961.
34. Vadukumpully S, Paul J, Mahanta N, Valiyaveettil S. Flexible conductive graphene/poly(vinyl chloride) composite thin films with high mechanical strength and thermal stability. Carbon. 2011; 49(1): 198–205.
35. Sanes J, Sánchez C, Pamies R, Avilés MD, Bermúdez MD. Extrusion of polymer nanocomposites with graphene and graphene derivative nanofillers: an overview of recent developments. Materials. 2020; 13(3): 549.
36. Batakliev T, Georgiev V, Kalupgian C, Muñoz PAR, Ribeiro H, Fechine GJM. Physico-chemical characterization of PLA-based composites holding carbon nanofillers. Appl. Compos. Mater. 2021; 28(4): 1175–1192.
37. Kang H, Kim DS. A study on the crystallization and melting of PLA nanocomposites with cellulose nanocrystals by DSC. Polymer Composites. 2023; 44(11): 7727–7736.
38. Standard PN-EN ISO 11357-(1-3):2016-2020 Tworzywa sztuczne - różnicowa kalorymetria skaningowa (DSC); Część 1: zasady ogólne; Część 2: wyznaczanie temperatury zeszklenia i stopnia przejścia w stan szklisty; Część 3: oznaczanie temperatury oraz entalpii topnienia i krystalizacji. Polish Committe for Standardization 2016–2020.
39. Standard PN-EN ISO 1133-1:2011 Tworzywa sztuczne - oznaczanie masowego wskaźnika szybkości płynięcia (MFR) i objętościowego wskaźnika szybkości płynięcia (MVR) tworzyw termoplastycznych - Część 1: metoda standardowa. Polish Committe for Standardization 2011.
40. Standard PN-EN ISO 294-1:2017 Tworzywa sztuczne - wtryskiwanie kształtek do badań z tworzyw termoplastycznych; Część 1: zasady ogólne, formowanie uniwersalnych kształtek do badań i kształtek w postaci beleczek. Polish Committe for Standardization 2017.
41. Standard PN-EN ISO 527-1:2020-01 Oznaczanie właściwości mechanicznych przy statycznym rozciąganiu; Część 1: zasady ogólne; Część 2: warunki badań tworzyw sztucznych przeznaczonych do prasowania wtrysku i wytłaczania. Polish Committe for Standardization 2012-2020.
42. Standard PN-EN ISO 179-1:2010 Tworzywa sztuczne. Oznaczanie udarności metodą Charpy'ego; Część 1: badanie nieinstrumentalne. Polish Committe for Standardization 2010.
43. Kotsilkova R, Tabakova S, Ivanova R. Effect of graphene nanoplatelets and multiwalled carbon nanotubes on the viscous and viscoelastic properties and printability of polylactide nanocomposites. Mech Time-Depend Mater. 2022; 26(3): 611–32.
44. Yadav N, Nain L, Khare SK. Studies on the degradation and characterization of a novel metal-free polylactic acid synthesized via lipase-catalyzed polymerization: a step towards curing the environmental plastic issue. Environmental Technology & Innovation. 2021; 24: 101845.
45. Yuniarto K, Purwanto YA, Purwanto S, Welt BA, Purwadaria HK, Sunarti TC. Infrared and Raman studies on polylactide acid and polyethylene glycol-400 blend. AIP Conference Proceedings. 2016; 1725(1): 020101.
46. Kister G, Cassanas G, Vert M. Effects of morphology, conformation and configuration on the IR and Raman spectra of various poly(lactic acid)s. Polymer. 1998; 39(2): 267–273.
47. Amorin NSQS, Rosa G, Alves JF, Gonçalves SPC, Franchetti SMM, Fechine GJM. Study of thermodegradation and thermostabilization of poly(lactide acid) using subsequent extrusion cycles. Journal of Applied Polymer Science. 2014; 131(6): 40023.
48. Adesina OT, Sadiku ER, Jamiru T, Ogunbiyi OF, Adesina OS. Thermal properties of spark plasma -sintered polylactide/graphene composites. Materials Chemistry and Physics. 2020; 242: 122545.
49. Ucpinar Durmaz B, Aytac A. Enhanced mechanical and thermal properties of graphene nanoplatelets-reinforced polyamide11/poly(lactic acid)

nanocomposites. Polymer Engineering & Science. 2023; 63(1): 105–117.

50. Kotsilkova R, Petrova-Doycheva I, Menseidov D, Ivanov E, Paddubskaya A, Kuzhir P. Exploring thermal annealing and graphene-carbon nanotube additives to enhance crystallinity, thermal, electrical and tensile properties of aged poly(lactic) acid-based filament for 3D printing. Composites Science and Technology. 2019; 181: 107712.
51. Xu Z, Niu Y, Yang L, Xie W, Li H, Gan Z, et al. Morphology, rheology and crystallization behavior of polylactide composites prepared through addition of five-armed star polylactide grafted multiwalled carbon nanotubes. Polymer. 2010; 51(3): 730–737.
52. Usachev SV, Lomakin SM, Koverzanova EV, Shilkina NG, Levina II, Prut EV. Thermal degradation of various types of polylactides research. The effect of reduced graphite oxide on the composition of the PLA4042D pyrolysis products. Thermochimica Acta. 2022; 712: 179227.
53. Ahmed J, Mulla MZ, Vahora A, Bher A, Auras R. Polylactide/graphene nanoplatelets composite films: impact of high-pressure on topography, barrier, thermal, and mechanical properties. Polymer Composites. 2021; 42(6): 2898–909.
54. Bartczak Z, Galeski A, Kowalczuk M, Sobota M, Malinowski R. Tough blends of poly(lactide) and amorphous poly([R,S]-3-hydroxy butyrate) – morphology and properties. European Polymer Journal. 2013; 49(11): 3630–3641.
55. Luyt AS, Gasmi S. Influence of blending and blend morphology on the thermal properties and crystallization behaviour of PLA and PCL in PLA/PCL blends. J Mater Sci. 2016; 51(9): 4670–4681.
56. Aliotta L, Gigante V, Geerinck R, Coltelli MB, Lazzeri A. Micromechanical analysis and fracture mechanics of poly(lactic acid) (PLA)/polycaprolactone (PCL) binary blends. Polymer Testing. 2023; 121: 107984.
57. Kumar S, Ramesh MR, Doddamani M, Rangappa SM, Siengchin S. Mechanical characterization of 3D printed MWCNTs/HDPE nanocomposites. Polymer Testing. 2022; 114: 107703.
58. Mysiukiewicz O, Barczewski M, Skórczewska K, Matykiewicz D. Correlation between processing parameters and degradation of different polylactide grades during twin-screw extrusion. Polymers. 2020; 12(6): 1333.
59. Kashi S, Gupta RK, Kao N, Hadigheh SA, Bhattacharya SN. Influence of graphene nanoplatelet incorporation and dispersion state on thermal, mechanical and electrical properties of biodegradable matrices. Journal of Materials Science & Technology. 2018; 34(6): 1026–1034.
60. Spinelli G, Kotsilkova R, Ivanov E, Petrova-Doycheva I, Menseidov D, Georgiev V. Effects of filament extrusion, 3D printing and hot-pressing on electrical and tensile properties of poly(Lactic) acid composites filled with carbon nanotubes and graphene. Nanomaterials. 2020; 10(1): 35.
61. Ren F, Li Z, Xu L, Sun Z, Ren P, Yan D. Large-scale preparation of segregated PLA/carbon nanotube composite with high efficient electromagnetic interference shielding and favourable mechanical properties. Composites Part B: Engineering. 2018; 155: 405–413.
62. Gonçalves C, Pinto A, Machado AV, Moreira J, Gonçalves IC, Magalhães F. Biocompatible reinforcement of poly(Lactic acid) with graphene nanoplatelets. Polymer Composites. 2018; 39(S1): E308–20.
63. Nimbagal V, Banapurmath NR, Sajjan AM, Patil AY, Ganachari SV. Studies on hybrid bio-nanocomposites for structural applications. J of Materi. Eng. and Perform. 2021; 30(9): 6461–6480.
64. Zou H, Yi C, Wang L, Liu H, Xu W. Thermal degradation of poly(lactic acid) measured by thermogravimetry coupled to Fourier transform infrared spectroscopy. J Therm Anal Calorim. 2009; 97(3): 929–935.
65. Beauson J, Schillani G, Van der Schueren L, Goutianos S. The effect of processing conditions and polymer crystallinity on the mechanical properties of unidirectional self-reinforced PLA composites, Composites Part A: Applied Science and Manufacturing. 2022; 152: 106668.